

1 ~~Towards understanding the intrinsic variations of the Priestley-Taylor~~  
2 ~~coefficient based on a theoretical derivation~~

3 Estimating the sensitivity of the Priestley-Taylor coefficient to air  
4 temperature and humidity

5

6 Ziwei Liu, Hanbo Yang \*, Changming Li, Taihua Wang

7 State Key Laboratory of Hydro-science and Engineering, Department of Hydraulic  
8 Engineering, Tsinghua University, Beijing, China

9 *Correspondence to:* Hanbo Yang (yanghanbo@tsinghua.edu.cn)

10 **Abstract**

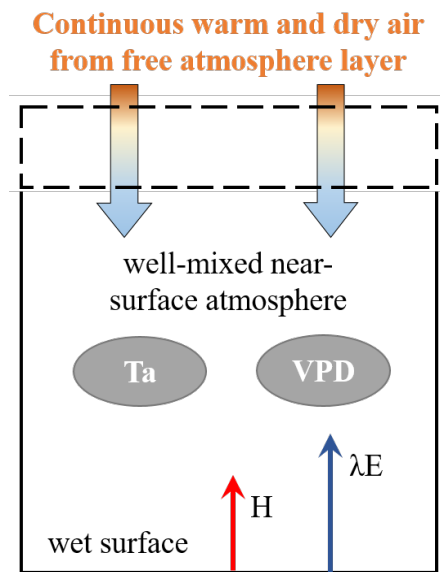
11 Priestley-Taylor (PT) coefficient ( $\alpha$ ) is generally set as a constant value or fitted as an  
12 empirical function of environmental variables, and it can bias the evaporation estimation  
13 or hydrological projections under global warming. By using an atmospheric boundary  
14 layer model, this study derives a theoretical and parameter-free equation for estimating  
15  $\alpha$  using an atmospheric boundary layer model, which shows that  $\alpha$  is as a function of  
16 air temperature (T) and specific humidity (Q). With observations from several water  
17 bodies and non-water-limited land sites, we demonstrate that in addition to well  
18 estimating the value of  $\alpha$ , the more importantly, the derived expressions can also well  
19 estimate capture the sensitivity of  $\alpha$  to T and Q, that is,  $d\alpha/dT$  and  $d\alpha/dQ$ , compared to  
20 water surface observations.  $\alpha$  is generally negatively associated with T and Q, of and its  
21 changes are which fundamentally controlled by T plays a more fundamental role in  
22 controlling  $\alpha$  behaviors and modulated by Q. Based on climate model data, it is shown we  
23 further show that the variation of this negative relationship between  $\alpha$  to and T (negative  
24 association) is of great importance for long-term hydrological predictions. We also  
25 provide For practical and broad uses, a lookup graph is also provided for practical and  
26 broad uses to directly find the values of  $d\alpha/dT$  and  $d\alpha/dQ$  values under specific conditions.  
27 Overall, Overall, the derived expression gives a physically clear and straightforward  
28 approach to quantify changes in  $\alpha$ , which is essential for PT-based hydrological  
29 simulation and projections.

30 **1. Introduction**

31 Evaporation from wet surfaces, including oceans, lakes, and reservoirs, is relevant to  
 32 global hydrological cycles and water availability. There is a long history of developing  
 33 theories and methods to estimate wet surface evaporation [Bowen, 1926; Penman, 1948;  
 34 Priestley and Taylor, 1972; Thornthwaite and Holzman, 1939; Yang and Roderick, 2019].  
 35 Among existing models, the Priestley-Taylor (PT) model/equation is known for its  
 36 transparent structure and low input requirement [Priestley and Taylor, 1972]. The PT  
 37 equation is widely used in evaporation estimation across varied scales and is the basis for  
 38 various hydrologic and land surface models. Specifically, the PT equation comes from  
 39 the equilibrium evaporation ( $\lambda E_{eq}$ ), and  $\lambda E_{eq}$  can be calculated as [Slatyer and McIlroy,  
 40 1961]:

41 
$$\lambda E_{eq} = \frac{\epsilon_a}{\epsilon_a + 1} (R_n - G) \quad (1)$$

42 where  $\lambda$  (**J/kg**) is the latent heat of water vaporization,  $\epsilon_a = \Delta/\gamma$ ,  $\Delta$  (**kPa/K**) is the slope of  
 43 the saturated vapor pressure versus temperature curve (a function of temperature), and  $\gamma$   
 44 is the psychrometric constant.  $\epsilon_a$  is a function of air temperature (T).  $R_n - G$  (**kPa/K**) is the  
 45 available energy. The equilibrium ~~condition~~ evaporation indicates that the near-surface  
 46 air is saturated, supposing the vapor pressure deficit (VPD) is zero. However, it does not  
 47 exist in the real world [Brutsaert and Stricker, 1979; J.P. Lhomme, 1997a], due to the  
 48 continuous exchanges of warm and dry air from the entrainment layer, although water is  
 49 continuously transported from the bottom wet surface into the atmosphere through  
 50 evaporation process (Figure 1).



51

52 Figure 1. Atmospheric boundary layer box model describing the energy and water fluxes  
 53 at the saturated surface and atmosphere above. The dotted line represents the removable  
 54 upper boundary of the box. H and  $\lambda E$  are the sensible and latent heat fluxes. Ta is the air

55 temperature and VPD is the vapor pressure deficit.

56  
57 In this case, the PT equation introduced a parameter,  $\alpha$ , known as the PT coefficient, to  
58 estimate wet surface evaporation [*Priestley and Taylor, 1972*].  $\alpha$  ~~includes-represents~~ the  
59 effects of vertical mixing of dry and moist air, and adjusts the equilibrium evaporation to  
60 the actual evaporation. So qualitatively speaking, the  $\alpha$  is impossibly lower than one  
61 because the air is always not saturated and can only infinitely close to saturated condition,  
62 no matter how moist the near-surface air is. The PT equation is:

$$63 \quad \lambda E = \alpha \frac{\epsilon_a}{\epsilon_a + 1} (R_n - G) \quad (2)$$

64 In the original study of *Priestley and Taylor* [1972], the value of  $\alpha$  is ~~fitted as~~ 1.26. ~~With~~  
65 ~~While the a~~ fixed  $\alpha$  value ~~of 1.26, the PT model~~ can reasonably estimate wet surface  
66 evaporation [*Yang and Roderick, 2019*]. ~~But, concurrently,~~ some studies found ~~that~~  $\alpha$   
67 ~~varies across time and space, for example,  $\alpha$~~  often shows a more prominent value under  
68 cold conditions and becomes lower as warms [*Debruin and Keijman, 1979; Xiao et al.,*  
69 *2020*]. This indicates that  $\alpha$  should ~~be a variable rather than not be~~ a constant ~~in space and~~  
70 ~~time~~ [*Maes et al., 2019*]. ~~Logically, this value would change with environmental~~  
71 ~~conditions, such as changes in temperature, humidity, advection, and dry-air entrainment~~  
72 [*Assouline et al., 2016; Crago et al., 2023; Eichinger et al., 1996; Guo et al., 2015; Jury*  
73 *and Tanner, 1975; J. P. Lhomme, 1997b; Maes et al., 2019; McNaughton and Spriggs,*  
74 *1986; van Heerwaarden et al., 2009*]. ~~However, the hydrology field predominantly~~  
75 ~~employs the fixed value of  $\alpha = 1.26$ , despite these earlier findings being over three~~  
76 ~~decades old.~~

77 ~~A~~ general method ~~for connecting  $\alpha$  to external factors to quantify the changes in  $\alpha$~~  is  
78 to inverse ~~it~~ with observations based on Equation (2) and then build relationships among  
79  $\alpha$  and investigated variables. ~~Since a~~ negative relationship between  $\alpha$  and temperature  
80 (T) is a consensus from multi-scale observations [*Assouline et al., 2016; Xiao et al.,*  
81 *2020*]. ~~Thus from the practical perspective,~~ many attempts empirically fitted  $\alpha$  as a  
82 function of ~~temperature T~~ [*Andreas and Cash, 1996; Hicks and Hess, 1977; Yang and*  
83 *Roderick, 2019*]. Recent work ~~further further~~ showed that the air humidity state ~~can also~~  
84 ~~influence the spatiotemporal patterns of also plays a role in  $\alpha$  changes~~ [*Su and Singh,*  
85 *2023*]. ~~While these methods promote our understanding of the potential variations in  $\alpha$ ,~~  
86 ~~they more lie on the empirical side and pay less attention to the underlying process. Hence,~~  
87 ~~various endeavors have been made to calculate  $\alpha$  through physical means, but they are~~  
88 ~~often constrained by the complexity of numerous parameters. For instance, in the research~~  
89 ~~conducted by J. P. Lhomme [1997b],  $\alpha$  was explicitly formulated utilizing the PM model~~  
90 ~~in conjunction with boundary layer theory. Nevertheless, these formulation incorporates~~  
91 ~~parameters that signify surface and aerodynamic resistances, making them hard to~~  
92 ~~determine through direct measurements. Subsequently, by using a refined boundary layer~~

93 ~~model, van Heerwaarden et al. [2009] Chiel C. van Heerwaarden et al.~~  
 94 ~~[2009b] introduced a mathematical expression for estimating  $\alpha$ , however, this expression~~  
 95 ~~also involves a set of parameters necessitating numerical experiments to delineate a~~  
 96 ~~feasible range for  $\alpha$ . Consequently, obtaining a precise  $\alpha$  estimation using conventional~~  
 97 ~~observations still has remained a challenge. Those findings help us to know how  $\alpha$  changes~~  
 98 ~~with external conditions. However, most works are on the empirical side and more about~~  
 99 ~~observed phenomena. Meanwhile, regarding physical understandings for  $\alpha$ , there still~~  
 100 ~~remain some questions, for example, why  $\alpha$  and  $T$  negatively correlate, how the~~  
 101 ~~interaction between temperature and air humidity affects  $\alpha$ , and whether  $\alpha$  has a lower~~  
 102 ~~boundary as it is negatively associated with temperature.~~

103 Based on a recent study by *Z Liu and Yang* [2021], here we aim to derive a physically  
 104 clear, explicit transparent, and physically clear equation to calibration-free equation for  
 105 estimating  $\alpha$ , by introducing a governing equation (potential vapor pressure deficit budget)  
 106 into the conventional boundary layer model. quantify relationships among  $\alpha$ ,  $T$ , and  $Q$ .  
 107 ~~The derived expression can be used to estimate the sensitivity of  $\alpha$  to  $T$  and  $Q$ .~~ In the  
 108 following sections, we will first provide the theory for estimating  $\alpha$  and its sensitivity to  
 109 climate conditions:  $T$  air temperature ( $T$ ) and humidity (represented by the air specific  
 110 humidity,  $Q$ ) $Q$ ., ~~then~~ we further evaluate the theory based on measurements from the  
 111 water and non-water-limited land surfaces measured data, followed by ~~an analysis of~~  
 112 ~~the influences of  $\alpha$  changes on long-term hydrologic projections.~~

## 113 2. Theory

### 114 2.1 Derivation of Bowen ratio

115 Here, we use an atmospheric boundary layer-based (ABL) model as the basis for the  
 116 Bowen ratio (defined as the ratio of sensible heat fluxes to latent heat fluxes,  $H/\lambda E$ )  
 117 derivation [*Z Liu and Yang*, 2021]. The fundamental conservation equations for states of  
 118 moisture and energy over the water surfaces are [*Raupach*, 2001]:

$$119 \quad \rho c_p \frac{d\theta}{dt} = \frac{H}{h} + \frac{\rho c_p g_e}{h} (\theta_e - \theta) \quad (3)$$

$$120 \quad \rho \lambda \frac{dQ}{dt} = \frac{\lambda E}{h} + \frac{\rho \lambda g_e}{h} (Q_e - Q) \quad (4)$$

121 where  $\theta$  (**K**) is the potential temperature,  $Q$  is the specific humidity,  $c_p$  (**J/kg/K**) is the  
 122 specific heat capacity of air at constant pressure,  $g_e$  (**m/s**) is the entrainment flux velocity  
 123 into the ABL box, and  $h$  (**m**) is the height of the ABL. The subscript  $e$  indicates the  
 124 variable is evaluated at the upper boundary of the ABL (see Figure 1).

125 According to Equations (3) and (4), we can obtain a formula to calculate the rate of VPD  
 126 (dVPD/dt, see details in *Z Liu and Yang [2021]*):

$$127 \quad \frac{dVPD}{dt} = \frac{\varepsilon_a H - \lambda E}{\rho \lambda h} + \frac{g_e}{h} \Delta_D \quad (5)$$

128 where  $\Delta_D$  is calculated as:

$$129 \quad \Delta_D = VPD_e - VPD \quad (6)$$

130 Under the ~~equilibrium~~ state that air is saturated, the water vapor is continuously  
 131 transported from the water surface to the atmosphere, keeping the air saturated. In this  
 132 case, there is no vertical moisture gradient, that is, the air near the surface and the air at  
 133 the upper boundary of the ABL should be saturated, so VPD and VPD<sub>e</sub> are both equal to  
 134 zero. With Equation ~~(6)~~(6), we can know  $\Delta_D = 0$ .

135 ~~Under the non-equilibrium state, the~~When air is not saturated, we can rewrite Equation  
 136 ~~(6)~~(6) as:

$$137 \quad \Delta_D = Q - Q_e + [Q_{sat}(\theta_e) - Q_{sat}(\theta)] \quad (7)$$

138 where Q<sub>e</sub> is much smaller than Q, and Q<sub>sat</sub>(θ<sub>e</sub>)-Q<sub>sat</sub>(θ) is small (one order of magnitude  
 139 smaller than Q), so the  $\Delta_D$  roughly equals Q [*Z Liu and Yang, 2021; Raupach, 2001*].

140 Under a relatively long-term (monthly and/or longer), there is a potential VPD budget  
 141 (dVPD/dt = 0) over water surfaces [*Raupach, 2001*], and g<sub>e</sub> can be estimated as the  
 142 function of H and λE as:

$$143 \quad g_e = \frac{H + \Lambda \cdot \lambda E}{\rho c_p \gamma_v h} \quad (8)$$

144 where Λ is a constant (0.07), and γ<sub>v</sub> is the potential virtual temperature gradient in the  
 145 free atmosphere above the ABL. γ<sub>v</sub>h can be set as a fixed value of 7 K [*Z Liu and Yang,*  
 146 *2021*]. Combining with the VPD budget, Equation (5) and ~~(8)~~(8), we can obtain the  
 147 expression for Bo:

$$148 \quad Bo = \begin{cases} \frac{1}{\varepsilon_a}, & \text{equilibrium} \\ \frac{1 - \Lambda \chi}{\varepsilon_a + \chi}, & \text{non-equilibrium} \end{cases} \quad (9)$$

149 where  $\chi = \frac{\lambda Q}{c_p \gamma_v h}$ , a function of Q.

150 **2.2 Theoretical formula for  $\alpha$**

151 The surface energy balance is expressed as:

152 
$$R_n = H + \lambda E + G = (1 + Bo)\lambda E + G. \quad (10)$$

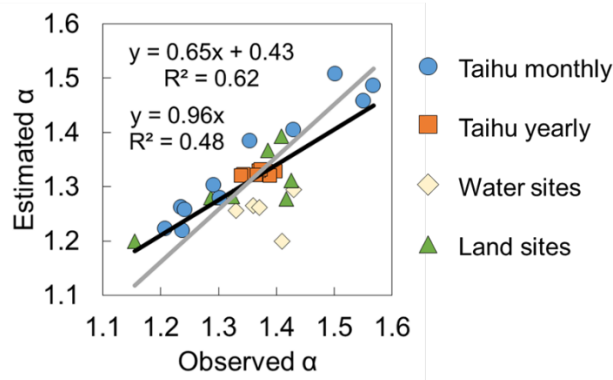
153 Combining Equations (2)(2) and (10)(10),  $\alpha$  can be calculated as:

154 
$$\alpha = \frac{1}{1 + Bo} \frac{\varepsilon_a + 1}{\varepsilon_a}. \quad (11)$$

155 With Equation (9)(9) and (11)(11), we can derive the formula for  $\alpha$ :

156 
$$\alpha = \begin{cases} 1, \text{ equilibrium} \\ 1 + \frac{(\varepsilon_a \Lambda + 1)\chi}{\varepsilon_a [\varepsilon_a + 1 + (1 - \Lambda)\chi]}, \text{ non-equilibrium} \end{cases} \quad (12)$$

157 Equation (12) is one of the main results in this study, and it can estimate  $\alpha$  well compared  
 158 to a large number of observations (Figure 2, please see the description of observed data  
 159 in Section 3).



160

161 Figure 2. Comparison between observed and Equation (12)(12) calculated  $\alpha$ . The black  
 162 line is the linear fitting with intercept and the gray line is the linear fitting through origin.  
 163 The observed  $\alpha$  is inversed by the PT model.

164 **2.3 The sensitivity of  $\alpha$  to air temperature and humidity**

165 According to the above derivations, we can know that  $\alpha$  is not a constant and it changes  
 166 with T and Q. The sensitivity of  $\alpha$  to T and Q,  $d\alpha/dT$  and  $d\alpha/dQ$ , determines the variation  
 167 of  $\alpha$  if the initial  $\alpha$  value is given. In this section, we derive explicit equations to estimate  
 168  $d\alpha/dT$  and  $d\alpha/dQ$ .

169 Firstly, we decompose  $\alpha$  changes in that of T and Q with partial differential equations  
 170 based on Equation (11)(11):

$$171 \quad \frac{\partial \alpha}{\partial T} = -\frac{1}{(1 + \text{Bo}_{\text{ABL}})^2} \frac{\varepsilon_a + 1}{\varepsilon_a} \frac{\partial \text{Bo}_{\text{ABL}}}{\partial T} - \frac{1}{\varepsilon_a^2} \frac{1}{1 + \text{Bo}_{\text{ABL}}} \frac{\partial \varepsilon_a}{\partial T}, \quad (13)$$

$$172 \quad \frac{\partial \alpha}{\partial Q} = -\frac{1}{(1 + \text{Bo}_{\text{ABL}})^2} \frac{\varepsilon_a + 1}{\varepsilon_a} \frac{\partial \text{Bo}_{\text{ABL}}}{\partial Q}, \quad (14)$$

173 where  $\frac{\partial \text{Bo}_{\text{ABL}}}{\partial T}$  and  $\frac{\partial \text{Bo}_{\text{ABL}}}{\partial Q}$  can be estimated based on Equation [错误!未找到引用源。](#)

174 as:

$$175 \quad \frac{\partial \text{Bo}_{\text{ABL}}}{\partial T} = -\frac{1 - \Lambda \chi}{(\varepsilon_a + \chi)^2} \frac{\partial \varepsilon_a}{\partial T}, \quad (15)$$

$$176 \quad \frac{\partial \text{Bo}_{\text{ABL}}}{\partial Q} = -\frac{\Lambda \varepsilon_a + 1}{(\varepsilon_a + \chi)^2} \frac{\partial \chi}{\partial Q}. \quad (16)$$

177 where terms of  $\frac{\partial \varepsilon_a}{\partial T}$  and  $\frac{\partial \chi}{\partial Q}$  can be approximated as:

$$178 \quad \frac{\partial \varepsilon_a}{\partial T} = \frac{1}{\gamma} \frac{\partial \Delta}{\partial T}, \quad (17)$$

$$179 \quad \frac{\partial \chi}{\partial Q} = \frac{\lambda}{c_p \gamma_v h}, \quad (18)$$

180 where  $\Delta$  can be calculated as:

$$181 \quad \Delta = \frac{4098 e_s}{(T + 237.3)^2}. \quad (19)$$

182 Combining Equation [\(13\)\(13\)-\(18\)\(18\)](#), we can obtain:

$$183 \quad \frac{\partial \alpha}{\partial T} = \frac{1}{\gamma} \left[ \frac{1}{(1 + \text{Bo}_{\text{ABL}})^2} \frac{1 - \Lambda \chi}{(\varepsilon_a + \chi)^2} \frac{\varepsilon_a + 1}{\varepsilon_a} - \frac{1}{\varepsilon_a^2} \frac{1}{1 + \text{Bo}_{\text{ABL}}} \right] \frac{\partial \Delta}{\partial T} \quad (20)$$

$$184 \quad \frac{\partial \alpha}{\partial Q} = \frac{1}{(1 + \text{Bo}_{\text{ABL}})^2} \frac{\Lambda \varepsilon_a + 1}{(\varepsilon_a + \chi)^2} \frac{\varepsilon_a + 1}{\varepsilon_a} \frac{\lambda}{c_p \gamma_v h} \quad (21)$$

185 We can rewrite the Equation (20) as follows:

$$186 \quad \frac{\partial \alpha}{\partial T} = -\frac{1}{\gamma} \frac{\chi \left[ \varepsilon_a (\Lambda \varepsilon_a + 2) + \chi (1 - \Lambda) + 1 \right]}{(1 + \text{Bo}_{\text{ABL}})^2 (\varepsilon_a + \chi)^2 \varepsilon_a^2} \frac{\partial \Delta}{\partial T}, \quad (22)$$

187 The total differentiation of  $\alpha$  is:

$$188 \quad d\alpha = \frac{\partial \alpha}{\partial T} dT + \frac{\partial \alpha}{\partial Q} dQ, \quad (23)$$



189 thus  $\frac{d\alpha}{dT}$  and  $\frac{d\alpha}{dQ}$  can be written as:

$$190 \quad \frac{d\alpha}{dT} = \frac{\partial\alpha}{\partial T} + \frac{\partial\alpha}{\partial Q} \frac{dQ}{dT}, \quad (24)$$

$$191 \quad \frac{d\alpha}{dQ} = \frac{\partial\alpha}{\partial Q} + \frac{\partial\alpha}{\partial T} \frac{dT}{dQ}. \quad (25)$$

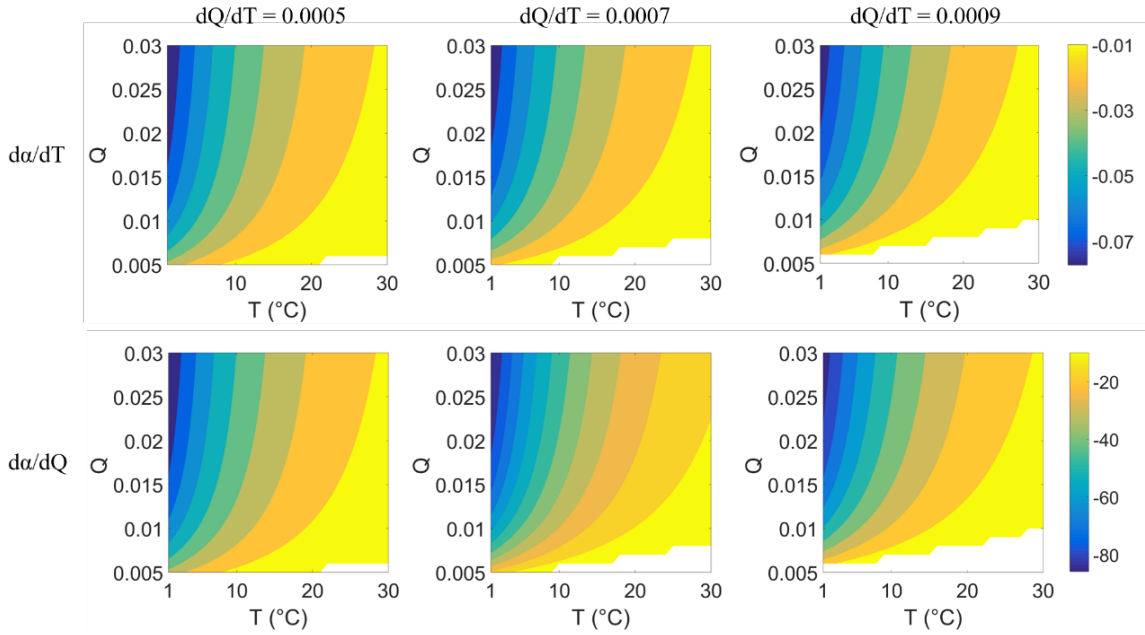
192 With the above equations, we can get theoretical relationships among  $\alpha$ , T, and Q. This  
 193 derivation can provide a simple and physically clear estimation for  $\alpha$  changes. We also  
 194 obtained  $d\alpha/dT$  and  $d\alpha/dQ$  values by fitting measured data using the linear regression  
 195 model.

196 For practical use, we simplified the Equation ~~(20)~~(20) and ~~(21)~~(21) as:

$$197 \quad \frac{\partial\alpha}{\partial T} = -\frac{1}{\gamma} \frac{\chi}{\epsilon_a} - \frac{1}{\chi} \frac{\partial\Delta}{\epsilon_a^2 \partial T} \quad (26)$$

$$198 \quad \frac{\partial\alpha}{\partial Q} = \frac{\epsilon_a + 1}{\epsilon_a (\epsilon_a + \chi + 1)^2} \frac{\chi}{Q} \quad (27)$$

199 We further gave a numerical plot to show how  $\alpha$  changes with T and Q (Figure 3). We  
 200 plot this figure by setting a  $dQ/dT$  gradient from 0.0005, 0.0007, and 0.0009/K to ensure  
 201 cover most of the cases over water surfaces. Figure 3 can be used as the lookup graphs to  
 202 directly find  $d\alpha/dT$  and  $d\alpha/dQ$  values. For example, for a water surface with  $dQ/dT$   
 203 about 0.0007 /K, the values of  $d\alpha/dT$  and  $d\alpha/dQ$  can be found in the second column  
 204 of Figure 3.



205

206 Figure 3. Values of  $da/dT$  and  $da/dQ$  under different  $T$  and  $Q$ . The first and second  
 207 rows are  $da/dT$  and  $da/dQ$ , respectively. The first to third columns are under different  
 208 correlations between  $Q$  and  $T$  ( $dQ/dT$ ) as 0.0005, 0.0007, and 0.0009/K, respectively.  
 209 The blank space in each subpanel refers to values of  $da/dT$  and  $da/dQ$  are negative,  
 210 indicating situations that rarely happen in the real world (i.e., with a very high temperature,  
 211 the specific humidity is hardly deficient over wet surfaces).

### 212 3. Cases and applications

#### 213 3.1 Data

214 We select data from eddy covariance measurements on several water surfaces [*Han and*  
 215 *Guo, 2023*]: (i) Lake Taihu, located in the Yangtze River Delta, China, with an area of  
 216  $\sim 2,400$  km<sup>2</sup>, an average depth of 1.9 m [*Lee et al., 2014*]. There are five sites over the  
 217 Taihu surface, and the poor-quality data marked with quality flags are removed. (ii) Lake  
 218 Poyang, located in the Yangtze Plain, China, with an area of  $\sim 3,000$  km<sup>2</sup> and an average  
 219 depth of 8.4 m [*X Zhao and Liu, 2018*]. (iii) Erhai, located in the Yun-Gui Plateau of  
 220 China, with an area of  $\sim 250$  km<sup>2</sup> and an average depth of 10 m [*Du et al., 2018*]. (iv)  
 221 Guandu Ponds, located in Anhui Province, China, with an area of  $\sim 0.05$  km<sup>2</sup> and an  
 222 average depth of 0.8 m [*J Zhao et al., 2019*]; (v) Lake Suwa, located in Nagano, Japan,  
 223 with an area of  $\sim 13$  km<sup>2</sup> and an average depth of 4 m [*Taoka et al., 2020*]. Months with  
 224 negative values of sensible heat fluxes have not remained. The latitude, longitude, and  
 225 available data period of five lakes/ponds are listed in Table 1. For  $\alpha$  changes in time, we  
 226 use data from Lake Taihu for investigation due to its sufficient data length. For  $\alpha$  changes  
 227 in space, we calculate the average temperature, specific humidity, and  $\alpha$  of each lake for  
 228 comparison.

229

Table 1. Location and date period of each water body.

Site	Lat (°)	Lon (°)	Size (km <sup>2</sup> )	Periods <sup>a</sup>	Sample size (number of months)
Taihu	31.23	120.11	3000	2012.01 - 2018.12	341 <sup>b</sup>
Poyang	29.08	116.40	2400	2013.08 - 2017.09	41
Erhai	25.77	100.17	250	2012.01 - 2018.12	24 <sup>c</sup>
Guandu	31.97	118.25	0.05	2017.06 - 2019.12	31
Suwa	36.05	138.11	13	2016.01 - 2018.12	36

230

231

232

233

Note: a. Periods refer to the date of the first measurement to the date of the last one, including months for which no data are available. b. There are five eddy covariance sites over lake Taihu. c. Only climatology monthly data from two periods of 2012-2015 and 2015-2018 are available.

234

235

236

237

238

239

240

241

242

243

244

245

246

247

248

249

Observations from global flux sites (FluxNet2015 database) are also selected. We first examine days without water stress based on the following steps [Maes *et al.*, 2019]. At each site, the evaporative fraction EF (i.e., latent heat flux over the sum of latent and sensible fluxes) is first calculated, and the days with EF exceeding the 95th percentile EF and with EF larger than 0.8 remain. Secondly, the days with soil moisture lower than 50% of the maximum soil moisture (taken as the 98th percentile of the soil moisture series) are removed. Days having rainfall and negative values of latent and sensible heat fluxes are also not included. As a result, a total of ~700 non-water-stressed site-days pass the criterion. Data is divided into seven vegetation types including croplands (CRO), wetlands (WET), evergreen needleleaf and mixed forests (DNF\_MF), evergreen broadleaf and deciduous broadleaf forests (EBF\_DBF), grasslands (GRA), close shrublands (CSH), and woody savanna (WSA), to analyze  $\alpha$  changes in space. It should be noted that we do not average the daily data to a monthly scale due to variations in data sizes across different months for a specific site. Instead, we organize the selected daily data by vegetation types, as the primary objective of utilizing land fluxes data is to assess the derived relationship spatially rather than temporally.

250

251

252

253

254

We also collect ocean surface data from 11 CMIP6 models (under scenario SSP585, Table 2) from 2021-2100 to see the temporal changes in  $\alpha$ . The calculation is limited to the latitudinal range 60°S to 60°N, and takes all ocean surface grids as a whole [Roderick *et al.*, 2014]. We average the monthly data to the yearly scale and calculate  $\alpha$  every ten years from 2021 to 2100 (i.e., 2021-2030, 2031-2040, etc.).

255

Table 2. CMIP6 models used in this study.

Model	Nation	Institute
ACCESS-ESM1-5	Australia	CSIRO
CanESM5	Canada	CCCma
CESM2-WACCM	USA	NCAR

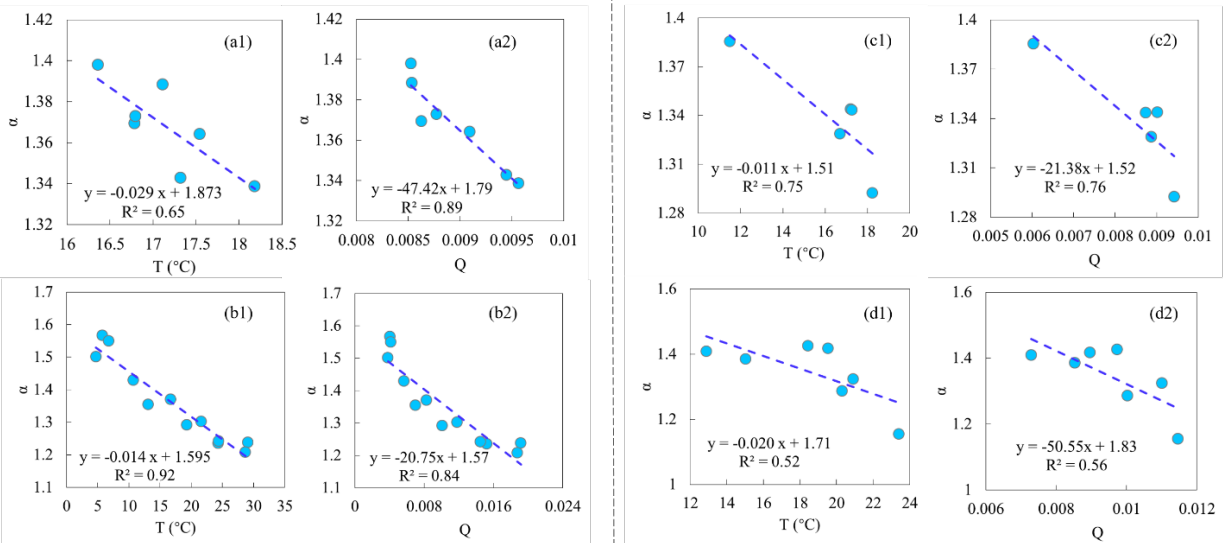
CMCC-CM2-SR5	Italy	CMCC
CMCC-ESM2	Italy	CMCC
FGOALS-g3	China	CAS
FIO-ESM-2-0	China	CAS
MPI-ESM1-2-HR	Germany	MPI-M
MPI-ESM1-2-LR	Germany	MPI-M
NorESM2-LM	Norway	NCC
NorESM2-MM	Norway	NCC

256 Note: CSIRO: Commonwealth Scientific and Industrial Research Organization;  
 257 CCCma: Canadian Centre for Climate Modelling and Analysis; NCAR: National Center  
 258 for Atmospheric Research; CMCC: Euro-Mediterranean Center on Climate Change;  
 259 CAS: Chinese Academy of Sciences; MPI-M: Max Planck Institute for Meteorology;  
 260 NCC: Norwegian Climate Centre.

### 261 3.2 Results

#### 262 (1) Temporal and spatial changes in $\alpha$

263 We used yearly and climatology monthly (from Jan to Dec) data from Lake Taihu to  
 264 investigate the temporal variation in  $\alpha$ .  $\alpha$  is firstly inversed by the PT model and  
 265 measurements, and then we found significant negative relationships of  $\alpha$  with both T and  
 266 Q (Figure 4). On the yearly scale, the regressed values of  $d\alpha/dT$  and  $d\alpha/dQ$  are -  
 267 0.029/°C and -47.42, and the values on the seasonal scale are -0.014/°C and -20.75,  
 268 respectively.  $d\alpha/dT$  on the seasonal scale is higher than that on the yearly scale because  
 269 the variation range of  $\alpha$  on the seasonal scale is more extensive. Theoretical derived  $d\alpha/dT$   
 270 and  $d\alpha/dQ$  roughly match with the regressed values (Table 3). We also analyzed on the  
 271 ten-day scale and obtained robust results (Figure S1 and Table S1).



272  
 273 Figure 4. Temporal and spatial relationships of  $\alpha$  and temperature (T) and specific  
 274 humidity (Q). (a-b) Temporal relationships based on lake Taihu data: (a) yearly data, and

275 (b) climatology monthly data. (c-d) Spatial relationships: (c) data from five water surface  
 276 sites, and (d) land surface data from FluxNet2015, each circle representing one vegetation  
 277 type. The linear regression line and correlation coefficient ( $R^2$ ) are shown in each  
 278 subpanel.

279

280 Table 3 Sensitivity of  $\alpha$  to temperature (T) and specific humidity (Q) by regression and  
 281 theoretical derivation.

		$d\alpha/dT$ ( $^{\circ}C$ )		$d\alpha/dQ$	
		regression	derivation	regression	derivation
Temporal	yearly	-0.029	-0.023	-47.42	-37.95
	seasonally	-0.014	-0.011	-20.75	-18.38
Spatial	water sites	-0.011	-0.012	-21.38	-24.30
	land sites	-0.020	-0.016	-50.55	-40.47

282

283 Spatial relationships of  $\alpha$  with T and Q are similar to that in time, i.e., higher T and Q  
 284 generally correspond to lower  $\alpha$ , supported by measurements over both water and land  
 285 surfaces (Figure 4). For the water surfaces, the values of  $d\alpha/dT$  and  $d\alpha/dQ$  are -  
 286  $0.011/^{\circ}C$  and -21.38, and the values for land surfaces are  $-0.020/^{\circ}C$  and -50.55. The  
 287 derived  $d\alpha/dT$  and  $d\alpha/dQ$  reasonably match well with the regressed values (Table 3).  
 288 The correlations (represented by  $R^2$  in Figure 4) between  $\alpha$  and T,  $\alpha$  and Q of water  
 289 surfaces are higher than those over the land surfaces. This indicates that changes in  $\alpha$  are  
 290 more associated with T and Q over water surfaces, which may be because T and Q  
 291 dominate the water surface evaporation process, while some other factors, like vegetation  
 292 and wind speed, also play specific roles over land surfaces.

293 Based on Equation (20) to (22),  $\partial\alpha/\partial T$  is always a negative value, and  $\partial\alpha/\partial Q$  is  
 294 always positive. The regressed and derived  $d\alpha/dT$  and  $d\alpha/dQ$  are both negative.  
 295 Combined with Equations (24), (25) and the positive relationship between T and Q, the  
 296  $\partial\alpha/\partial T$  plays a more critical role in determining (the signs of)  $d\alpha/dT$  and  $d\alpha/dQ$ , that  
 297 is,  $|\partial\alpha/\partial T| > \partial\alpha/\partial Q \cdot dQ/dT$  and  $|\partial\alpha/\partial T \cdot dT/dQ| > \partial\alpha/\partial Q$ . Specifically, based on the data  
 298 from lake Taihu (for detecting  $\alpha$  changes in time) and data from different water surface  
 299 sites and land surface sites (for detecting  $\alpha$  changes in space), we found the contribution  
 300 of  $\partial\alpha/\partial T \cdot dT$  to  $d\alpha$  is  $\sim 70\%$ , much more significant than that of  $\partial\alpha/\partial Q \cdot dQ$  of  $\sim 30\%$   
 301 (Table 4). Therefore, according to the evaporation process over the wet surface (Section  
 302 2.1) and the above analyses, we can conclude that  $\alpha$  is fundamentally controlled by T and  
 303 modulated by Q.

304 Table 4. Contributions of changes in temperature (T) and specific humidity (Q) to  
 305 changes in  $\alpha$ .

		$d\alpha$	contribution of $\frac{\partial\alpha}{\partial T}dT$	contribution of $\frac{\partial\alpha}{\partial Q}dQ$
Temporal	yearly	-0.035	78%	22%
	seasonally	-0.256	67%	33%
Spatial	water sites	-0.081	68%	32%
	land sites	-0.167	77%	23%
Average		----	72.5%	27.5%

306 Note: Since  $d\alpha = \frac{\partial\alpha}{\partial T}dT + \frac{\partial\alpha}{\partial Q}dQ$ , the contribution of  $\frac{\partial\alpha}{\partial T}dT$  is calculated as

307  $\left| \frac{\frac{\partial\alpha}{\partial T}dT}{\frac{\partial\alpha}{\partial T}dT + \frac{\partial\alpha}{\partial Q}dQ} \right|$ , and is the contribution of  $\frac{\partial\alpha}{\partial Q}dQ$  calculated as

308  $\left| \frac{\frac{\partial\alpha}{\partial Q}dQ}{\frac{\partial\alpha}{\partial T}dT + \frac{\partial\alpha}{\partial Q}dQ} \right|$ .  $d\alpha$  refers to the estimated variation of  $\alpha$  from lowest to highest

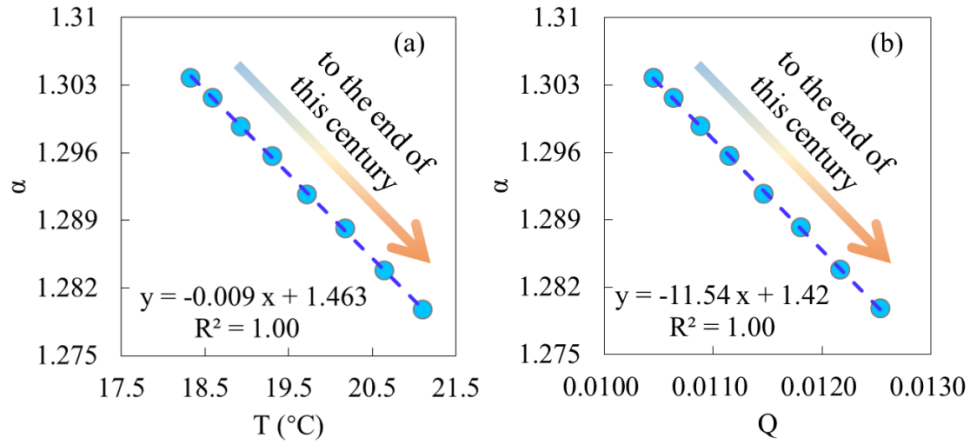
309 T (also from lowest to highest Q since T and Q are positively correlated).

310 Derived  $d\alpha/dT$  and  $d\alpha/dQ$  have more or less errors compared to the regressed values.  
 311 Several reasons can explain this: (i) errors in measurements of eddy covariance systems;  
 312 (ii) the additional factors other than T and Q, like wind speed, can also influence  $\alpha$ ; (iii)  
 313 the relationship of  $\alpha$  and T (also  $\alpha$  and Q) cannot be well represented by the linear  
 314 regression model. Besides, the water surface size effects on evaporation and  $\alpha$ , reported  
 315 by *Han and Guo* [2023], are not well considered in the presented derivation. Nevertheless,  
 316 the derived expression can fairly match the observations of water bodies with various  
 317 sizes (Table 3).

## 318 (2) Potential applications for global projections

319 Based on CMIP6 ocean surface data, we also detected significant negative relationships  
 320 of  $\alpha$  with T and Q (Figure 5).  $d\alpha/dT$  and  $d\alpha/dQ$  obtained by the linear regression are -  
 321 0.009/°C and -11.54, respectively. The derived  $d\alpha/dT$  and  $d\alpha/dQ$  are close to the  
 322 regressed value as -0.009/°C and -10.74. We further compared the changes in T, Q, and  
 323 heat fluxes between the first and the last ten years in 2021-2100 (Table 5). To the end of  
 324 this century, CMIP6 models predict that ocean average available energy ( $R_n-G$ ) and latent  
 325 heat flux (also evaporation) will increase by  $\sim 3.1$  W/m<sup>2</sup> and  $\sim 6.0$  W/m<sup>2</sup>, respectively.  
 326 Using the PT model with the fixed  $\alpha$  (1.26), predicted evaporation shows an increase of  
 327  $\sim 8.0$  W/m<sup>2</sup>, far higher than climate models' direct output (with a relative bias of  $\sim 30\%$ ).  
 328 Based on derived  $\alpha$ , ocean evaporation shows a much smaller increase of  $\sim 5.8$  W/m<sup>2</sup>, with  
 329 less than 5% relative bias compared to CMIP6 values (Figure 6). This indicates that  
 330 changes in  $\alpha$  should be well considered for the long-term projections. So here we suggest  
 331 introducing the negative relationship between  $\alpha$  and T, proposed in this study, into the

332 original PT model to correct for the overestimated sensitivity of evaporation to  
 333 temperature [Z Liu *et al.*, 2022], which could also improve the reliability of global long-  
 334 term drought predictions [Greve *et al.*, 2019].

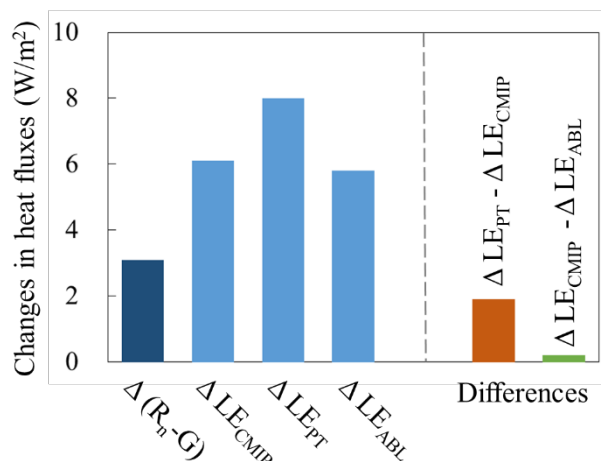


335  
 336 Figure 5. Temporal relationship of (a)  $\alpha$  and temperature (T), and (b)  $\alpha$  and specific  
 337 humidity (Q) over global ocean surfaces. Each dot denotes the data in each 10-year  
 338 window (2021-2030, 2031-2041, ..., 2091-2100), from left to right is from 2021-2030 to  
 339 2091-2100.

340  
 341 Table 5. Ocean surface temperature, specific humidity, and heat fluxes at the first ten  
 342 years (2021-2030) and the end of the 21<sup>st</sup> century (2091-2100). T, Q,  $R_n-G$ , and LE are  
 343 direct outputs of climate models.  $\alpha$ -CMIP refers to  $\alpha$  inverted by the PT model with CMIP  
 344 data.  $LE_{PT}$  is calculated by the PT model with fixed  $\alpha$  at 1.26.  $\alpha$ -ABL refers to  $\alpha$  estimated  
 345 by the ABL model.  $LE_{ABL}$  is calculated by the PT model with  $\alpha$ -ABL.

Period	T (°C)	Q (-)	$R_n-G$ (W/m <sup>2</sup> )	LE (W/m <sup>2</sup> )	$\alpha$ -CMIP	$LE_{PT}$ (W/m <sup>2</sup> )	$\alpha$ -ABL	$LE_{ABL}$ (W/m <sup>2</sup> )
2021-2030	18.1	0.010	122.9	106.8	1.304	103.2	1.316	107.7
2091-2100	21.1	0.013	126.0	112.9	1.279	111.2	1.287	113.5
$\Delta$	3.0	0.003	3.1	6.1	-0.025	8.0	-0.029	5.8

346



347  
348 Figure 6. Stylized diagram showing the average changes in heat fluxes over global  
349 ocean surfaces.

#### 350 4. Discussions and Conclusions

351 In this study, we employed an open boundary layer model with a An atmospheric  
 352 boundary layer model governing potential VPD budget [Raupach, 2000; 2001], originally  
 353 built integrated –initially on by Z Liu and Yang [2021], was used to formulate derive an  
 354 expression for the Priestley-Taylor coefficient,  $\alpha$ . Notably, the governing equation allows  
 355 the derived expression has no calibrated parameters and can estimate a precise  $\alpha$  value  
 356 with normal observations, rendering it superior to other methods that also built with the  
 357 boundary layer theory [J. P. Lhomme, 1997b; Chiel C. van Heerwaarden et al., 2009]. [J.  
 358 P. Lhomme, 1997b; Chiel C. van Heerwaarden et al., 2009b] With the expression and a  
 359 variety of measurements, we further demonstrated that The expression explicitly shows  
 360 the dependences of  $\alpha$  on air temperature and specific humidity. temperature exerts a more  
 361 significant influence on variations in  $\alpha$ , as opposed to specific humidity Temperature  
 362 changes dominate changes in  $\alpha$ , compared to specific humidity. We suggest that for  
 363 studies focusing on evaporation and/or drought projections, it is crucial to thoroughly  
 364 characterize the negative correlation between  $\alpha$  and temperature, a relationship easily  
 365 determined using the derived expression. for the study focusing on evaporation and/or  
 366 drought projections, the negative relationship between  $\alpha$  and temperature should be well  
 367 characterized, which can be calculated by the proposed expression.

368 It should be noted that except for the PT model, the PM-based model can be also used  
 369 to estimate wet surface evaporation [Penman, 1948; Shuttleworth, 1993]. While PM-based  
 370 equations encapsulate all processes that possibly affect evaporation, the PT model, taking  
 371 evaporation as a simple function of radiation and temperature, takes more account of the  
 372 feedback/balance between the surface and near atmosphere (Figure 1). Besides, it has  
 373 been noted that the PM-based models may fail at certain limits, and cannot capture the  
 374 sensitivity of evaporation to temperature changes (Liu et al., 2022; McColl, 2020). So in

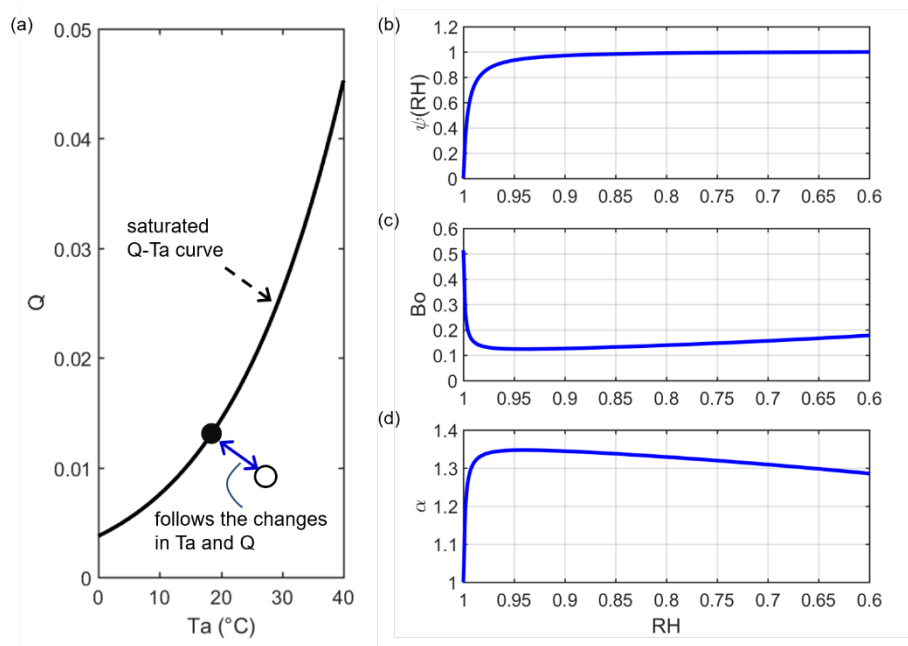


375 this case, also with the fact that the PT model is currently one of the most popular  
 376 equations due to its low input requirements, revisiting this classic model can greatly  
 377 promote its adaption under the changing climate.

378 In Section 2.1, it was suggested that  $\Delta_D = 0$  for the ~~equilibrium states~~ saturated air while  
 379  $\Delta_D \approx Q$  for the non-~~equilibrium states~~ saturated air. In theory, it is expected that the  
 380 transition track between saturated equilibrium and non-saturated equilibrium states  
 381 should be continuous and smooth. That is, the changes in the value of  $\Delta_D$  between the  
 382 saturated equilibrium state (0) and non-saturated (Q) equilibrium states ( $\ominus$ ) should follow  
 383 the variations in air energy and moisture (Figure 7). Since the relative humidity (RH)  
 384 includes both information on air temperature and humidity, here we introduce a possible  
 385 track of  $\Delta_D$  depending on RH as:  $\Delta_D = \psi(\text{RH}) \cdot Q$ . As we expect, the value of  $\Delta_D$   
 386 approaches 0 when the air is very moist (i.e., very close to the saturated equilibrium state  
 387 and RH close to 1), so  $\psi$  should be a nonlinear and monotone convex function of RH.  
 388 We give a possible expression of  $\psi(\text{RH})$  as:

$$389 \quad \psi(\text{RH}) = 1 - \frac{1}{1 + m \times \left( \frac{\text{RH}_{\max} - \text{RH}}{\text{RH} - \text{RH}_{\min}} \right)^n} \quad (28)$$

390 where  $\text{RH}_{\max}$  is 1, and  $\text{RH}_{\min}$  is 0.6 [McColl and Tang, 2023] over the water surfaces.  $m$   
 391 and  $n$  are shape parameters. To make  $\psi(\text{RH})$  simple, we fixed  $n$  at 1, and let  $m$  be 100.  
 392 The relationship between  $\psi(\text{RH})$  and RH can be viewed in Figure 7 (b). For a specific  
 393 case that  $T$  at 18 °C, we show the changes in  $\text{Bo}$  and  $\alpha$  with RH in Figure 7 (c)-(d).  
 394 Although there is a dramatic shift in  $\text{Bo}$  or  $\alpha$ , it appears when RH is at 0.95-1, which is  
 395 outside the vast majority of actual cases (RH is generally smaller than 0.9 on a monthly  
 396 or longer scale). After the shift point, with RH decreases,  $\psi(\text{RH})$ ,  $\text{Bo}$ , and  $\alpha$  remain  
 397 roughly stable. It is worth noting that Equation (28)(28) (with specific parameters) is one  
 398 possible case that connects the transition between saturated equilibrium and non-saturated  
 399 air equilibrium states, a fine determination may be affected by local conditions, but  $\Delta_D$   
 400 value around  $Q$  is expected for most of the cases.



401

402 Figure 7. (a) Transition between saturated equilibrium and non-saturated air equilibrium  
 403 states. The filled circle represents one case in which the air is saturated (saturated  
 404 equilibrium state) and the open circle represents one case in which air is not saturated  
 405 (non- saturated equilibrium state). (b) Relationship between  $\psi(RH)$  and  $RH$  with  
 406 Equation (28)(28). (c)-(d) Changes in  $B_0$  and  $\alpha$  as the function of  $RH$  when air  
 407 temperature is fixed at 18 °C.

408 We recommend utilizing the derived model under warm conditions, for example, when  
 409 the air temperature exceeds zero, to account for the prerequisite of a well-mixed boundary  
 410 layer. In extremely cold regions or seasons, the water surface temperature can be lower  
 411 than the air temperature, resulting in a downward sensible heat flux [de Bruin, 1982].  
 412 Under such circumstances, the boundary layers exhibit relative stability and may not  
 413 reach a well-mixed state. Additionally, we advise adopting a temporal scale ranging from  
 414 weekly to monthly when applying the derived model. This is because the potential VPD  
 415 budget (the governing equation) may not be rapidly achieved, such as on a diurnal or daily  
 416 basis. Furthermore, over a longer term, the sensible heat flux typically manifests as  
 417 upward in the majority of scenarios than on a fine temporal scale.

418 The derived formula for  $\alpha$  has important practical meanings. For example, it would be  
 419 useful for estimating water surface evaporation and actual evapotranspiration based on  
 420 the PT model [Maes et al., 2019; Miralles et al., 2011]. It can also help to constrain the  
 421 relationships among  $\alpha$ ,  $T$ , and  $Q$  in the complementary relationship, whose performance  
 422 previously depended on the inversed  $\alpha$  [X Liu et al., 2016]. Besides, considering the  
 423 impacts of changing climate on  $\alpha$  can significantly improve the performance of the  
 424 hydrologic model in runoff simulations and predictions [Pimentel et al., 2023].

425 **Author Contributions**

426 Conceptualization: Ziwei Liu, Hanbo Yang. Data curation: Ziwei Liu. Formal analysis:  
427 Ziwei Liu. Funding acquisition: Hanbo Yang. Methodology: Ziwei Liu, Hanbo Yang.  
428 Software: Ziwei Liu. Supervision: Hanbo Yang. Writing – original draft: Ziwei Liu.  
429 Writing – review & editing: Changming Li, Taihua Wang, Hanbo Yang.

430 **Data availability**

431 Data of Lake Taihu can be obtained from Harvard Dataverse,  
432 <https://doi.org/10.7910/DVN/HEWCWM>. The data of Poyang Lake can be obtained  
433 from *X Zhao and Liu* [2018] and *Gan and Liu* [2020]. The data of Erhai can be obtained  
434 from *Du et al.* [2018]. The data of Guandu can be obtained from *J Zhao et al.* [2019].  
435 The data of Suwa lake can be obtained from the AsiaFlux  
436 ([http://asiaflux.net/index.php?page\\_id=1355](http://asiaflux.net/index.php?page_id=1355)). FluxNet 2015 data are available at  
437 <https://fluxnet.fluxdata.org/data/download-data/>. CMIP6 data can be obtained from  
438 Earth System Grid Federation (<https://esgf-node.llnl.gov>).

439 **Acknowledgments**

440 This study is financially supported by the National Natural Science Foundation of China  
441 (grant nos. 51979140, 42041004).

442 **References:**

- 443 Andreas, E. L., and B. A. Cash (1996), A new formulation for the Bowen ratio over saturated surfaces,  
444 *Journal of Applied Meteorology*, 35(8), 1279-1289, doi:10.1175/1520-  
445 0450(1996)035<1279:anfftb>2.0.co;2.
- 446 Assouline, S., D. Li, S. Tyler, J. Tanny, S. Cohen, E. Bou-Zeid, M. Parlange, and G. G. Katul (2016), On  
447 the variability of the Priestley-Taylor coefficient over water bodies, *Water Resources Research*, 52(1), 150-  
448 163, doi:10.1002/2015wr017504.
- 449 Bowen, I. S. (1926), The ratio of heat losses by conduction and by evaporation from any water surface,  
450 *Physical Review*, 27(6), 779-787, doi:10.1103/PhysRev.27.779.
- 451 Brutsaert, W., and H. J. W. r. r. Stricker (1979), An advection-aridity approach to estimate actual regional  
452 evapotranspiration, 15(2), 443-450.
- 453 Crago, R. D., J. Szilagyi, and R. J. Qualls (2023), What is the Priestley–Taylor wet-surface evaporation  
454 parameter? Testing four hypotheses, *Hydrol. Earth Syst. Sci.*, 27(17), 3205-3220, doi:10.5194/hess-27-  
455 3205-2023.
- 456 de Bruin, H. A. R. (1982), Temperature and energy balance of a water reservoir determined from standard  
457 weather data of a land station, *Journal of Hydrology*, 59(3), 261-274, doi:[https://doi.org/10.1016/0022-  
458 1694\(82\)90091-9](https://doi.org/10.1016/0022-1694(82)90091-9).
- 459 Debruin, H. A. R., and J. Q. Keijman (1979), PRIESTLEY-TAYLOR EVAPORATION MODEL APPLIED  
460 TO A LARGE, SHALLOW LAKE IN THE NETHERLANDS, *Journal of Applied Meteorology*, 18(7),  
461 898-903, doi:10.1175/1520-0450(1979)018<0898:Tptema>2.0.Co;2.
- 462 Du, Q., H. Z. Liu, Y. Liu, L. Wang, L. J. Xu, J. H. Sun, and A. L. Xu (2018), Factors controlling evaporation  
463 and the CO<sub>2</sub> flux over an open water lake in southwest of China on multiple temporal scales, *International  
464 Journal of Climatology*, 38(13), 4723-4739, doi:10.1002/joc.5692.
- 465 Eichinger, W. E., M. B. Parlange, and H. Stricker (1996), On the concept of equilibrium evaporation and  
466 the value of the Priestley-Taylor coefficient, *Water Resources Research*, 32(1), 161-164.
- 467 Gan, G., and Y. Liu (2020), Heat Storage Effect on Evaporation Estimates of China's Largest Freshwater  
468 Lake, 125(19), e2019JD032334, doi:<https://doi.org/10.1029/2019JD032334>.
- 469 Greve, P., M. L. Roderick, A. M. Ukkola, and Y. Wada (2019), The aridity Index under global warming,  
470 *Environmental Research Letters*, 14(12), doi:10.1088/1748-9326/ab5046.
- 471 Guo, X., H. Liu, and K. J. B.-L. M. Yang (2015), On the application of the Priestley–Taylor relation on sub-  
472 daily time scales, 156, 489-499.
- 473 Han, S., and F. Guo (2023), Evaporation From Six Water Bodies of Various Sizes in East Asia: An Analysis  
474 on Size Dependency, *Water Resources Research*, 59(6), doi:10.1029/2022wr032650.
- 475 Hicks, B. B., and G. D. Hess (1977), On the Bowen Ratio and Surface Temperature at Sea, *Journal of  
476 Physical Oceanography*, 7(1), 141-145, doi:10.1175/1520-0485(1977)007<0141:otbras>2.0.co;2.
- 477 Jury, W., and C. J. A. J. Tanner (1975), Advection Modification of the Priestley and Taylor  
478 Evapotranspiration Formula 1, 67(6), 840-842.
- 479 Lee, X., et al. (2014), THE TAIHU EDDY FLUX NETWORK An Observational Program on Energy, Water,  
480 and Greenhouse Gas Fluxes of a Large Freshwater Lake, *Bulletin of the American Meteorological Society*,  
481 95(10), 1583-1594, doi:10.1175/bams-d-13-00136.1.
- 482 Lhomme, J. P. (1997a), An examination of the Priestley-Taylor equation using a convective boundary layer  
483 model, *Water Resources Research*, 33(11), 2571-2578.

- 484 Lhomme, J. P. (1997b), A THEORETICAL BASIS FOR THE PRIESTLEY-TAYLOR COEFFICIENT,  
485 *Boundary-Layer Meteorology*, 82(2), 179-191, doi:10.1023/A:1000281114105.
- 486 Liu, X., C. Liu, and W. Brutsaert (2016), Regional evaporation estimates in the eastern monsoon region of  
487 China: Assessment of a nonlinear formulation of the complementary principle, 52(12), 9511-9521,  
488 doi:<https://doi.org/10.1002/2016WR019340>.
- 489 Liu, Z., J. Han, and H. Yang (2022), Assessing the ability of potential evaporation models to capture the  
490 sensitivity to temperature, *Agricultural and Forest Meteorology*, 317, 108886.
- 491 Liu, Z., and H. Yang (2021), Estimation of Water Surface Energy Partitioning With a Conceptual  
492 Atmospheric Boundary Layer Model, *Geophysical Research Letters*, 48(9), e2021GL092643,  
493 doi:<https://doi.org/10.1029/2021GL092643>.
- 494 Maes, W. H., P. Gentine, N. E. C. Verhoest, and D. G. Miralles (2019), Potential evaporation at eddy-  
495 covariance sites across the globe, *Hydrology and Earth System Sciences*, 23(2), 925-948, doi:10.5194/hess-  
496 23-925-2019.
- 497 McColl, K. A., and L. I. Tang (2023), An analytic theory of near-surface relative humidity over land,  
498 *Journal of Climate*, doi:<https://doi.org/10.1175/JCLI-D-23-0342.1>.
- 499 McNaughton, K., and T. Spriggs (1986), A MIXED-LAYER MODEL FOR REGIONAL EVAPORATION,  
500 *Boundary-Layer Meteorology*, 34(3), 243-262, doi:10.1007/bf00122381.
- 501 Miralles, D. G., T. Holmes, R. De Jeu, J. Gash, A. Meesters, A. J. H. Dolman, and E. S. Sciences (2011),  
502 Global land-surface evaporation estimated from satellite-based observations, 15(2), 453-469.
- 503 Penman, H. L. (1948), Natural evaporation from open water, bare soil and grass, *Proceedings of the Royal*  
504 *Society of London Series a-Mathematical and Physical Sciences*, 193(1032), 120-145,  
505 doi:10.1098/rspa.1948.0037.
- 506 Pimentel, R., B. Arheimer, L. Crochemore, J. C. M. Andersson, I. G. Pechlivanidis, and D. Gustafsson  
507 (2023), Which Potential Evapotranspiration Formula to Use in Hydrological Modeling World-Wide?, 59(5),  
508 e2022WR033447, doi:<https://doi.org/10.1029/2022WR033447>.
- 509 Priestley, C. H. B., and R. J. Taylor (1972), Assessment of surface heat-flux and evaporation using large-  
510 scale parameters, *Monthly Weather Review*, 100(2), 81-92, doi:10.1175/1520-  
511 0493(1972)100<0081:otaosh>2.3.co;2.
- 512 Raupach, M. R. (2000), Equilibrium evaporation and the convective boundary layer, *Boundary-Layer*  
513 *Meteorology*, 96(1-2), 107-141, doi:10.1023/a:1002675729075.
- 514 Raupach, M. R. (2001), Combination theory and equilibrium evaporation, *Quarterly Journal of the Royal*  
515 *Meteorological Society*, 127(574), 1149-1181, doi:10.1256/smsqj.57401.
- 516 Roderick, M. L., F. Sun, W. H. Lim, and G. D. Farquhar (2014), A general framework for understanding  
517 the response of the water cycle to global warming over land and ocean, *Hydrology and Earth System*  
518 *Sciences*, 18(5), 1575-1589, doi:10.5194/hess-18-1575-2014.
- 519 Shuttleworth, W. J. (1993), Evaporation In: Maidment, DR Handbook of hydrology, edited, McGraw-Hill  
520 New York.
- 521 Slatyer, R. O., and I. C. McIlroy (1961), *Practical microclimatology: with special reference to the water*  
522 *factor in soil-plant-atmosphere relationships*, Melbourne: Commonwealth Scientific and Industrial  
523 Research Organisation.
- 524 Su, Q., and V. P. Singh (2023), Calibration-Free Priestley-Taylor Method for Reference Evapotranspiration  
525 Estimation, 59(3), e2022WR033198, doi:<https://doi.org/10.1029/2022WR033198>.
- 526 Taoka, T., H. Iwata, R. Hirata, Y. Takahashi, Y. Miyabara, and M. Itoh (2020), Environmental Controls of  
527 Diffusive and Ebullitive Methane Emissions at a Subdaily Time Scale in the Littoral Zone of a Midlatitude  
528 Shallow Lake, *Journal of Geophysical Research-Biogeosciences*, 125(9), doi:10.1029/2020jg005753.

- 529 Thornthwaite, C. W., and B. Holzman (1939), Evaporation from land and water surfaces, *Monthly Weather*  
530 *Review*, 67, 4-11, doi:10.1175/1520-0493(1939)67<4:tdoefl>2.0.co;2.
- 531 van Heerwaarden, C. C., J. V. G. de Arellano, A. F. Moene, and A. A. M. Holtslag (2009), Interactions  
532 between dry-air entrainment, surface evaporation and convective boundary-layer development, *Quarterly*  
533 *Journal of the Royal Meteorological Society*, 135(642), 1277-1291, doi:10.1002/qj.431.
- 534 Xiao, W., Z. Zhang, W. Wang, M. Zhang, Q. Liu, Y. Hu, W. Huang, S. Liu, and X. Lee (2020), Radiation  
535 Controls the Interannual Variability of Evaporation of a Subtropical Lake, *Journal of Geophysical*  
536 *Research-Atmospheres*, 125(8), doi:10.1029/2019jd031264.
- 537 Yang, Y., and M. L. Roderick (2019), Radiation, surface temperature and evaporation over wet surfaces,  
538 *Quarterly Journal of the Royal Meteorological Society*, 145(720), 1118-1129, doi:10.1002/qj.3481.
- 539 Zhao, J., et al. (2019), An evaluation of the flux-gradient and the eddy covariance method to measure CH<sub>4</sub>,  
540 CO<sub>2</sub>, and H<sub>2</sub>O fluxes from small ponds, *Agricultural and Forest Meteorology*, 275, 255-264,  
541 doi:10.1016/j.agrformet.2019.05.032.
- 542 Zhao, X., and Y. Liu (2018), Variability of Surface Heat Fluxes and Its Driving Forces at Different Time  
543 Scales Over a Large Ephemeral Lake in China, *Journal of Geophysical Research-Atmospheres*, 123(10),  
544 4939-4957, doi:10.1029/2017jd027437.

545